Supporting Information for

MnX (X=P, As, Sb) Monolayer: A New Type of 2D Intrinsic Room-Temperature Half-Metallicity with large anisotropy

Bing Wang, [‖,†] Yehui Zhang,[‖,†] Liang Ma, [†] Qisheng Wu,[ǂ] Xiwen Zhang, [‡] Yilv Guo,[†] and Jinlan Wang[†,§,*]

[†]School of Physics, Southeast University, Nanjing 211189, China

[‡]School of Mechanism Engineering & School of Physics, Southeast University, Nanjing 211189, China

[ǂ] Department of Chemistry and Chemical Biology, the University of New Mexico, USA

[§]Synergetic Innovation Center for Quantum Effects and Applications (SICQEA), Hunan Normal University, Changsha, Hunan 410081, China

Bing Wang and Yehui Zhang contributed equally.
*Correspondence should be addressed to: *J. Wang* (jlwang@seu.edu.cn)

Table of Contents

1. Computational methods:

Particle swarm optimization (PSO) algorithm as implemented in CALYPSO [1]was adapted to search for stable 2D monolayers[2-6]. In the first generation of the structure search, random structures were constructed and then these structures were optimized by using the first-principles method. After analyzing the first generation structures, a certain number of new structures (60% of the population size) were reserved to evolve into next generation by PSO. The other 40% of new generation structures were randomly constructed to guarantee the structure diversity. In our PSO simulations, the population size and number of generation were all set to be 30. We repeat it four times independently. For each PSO simulation, 900 structures were generated and tens of structures with lower energies were further optimized at PBE level of theory using Vienna ab initio simulation package.

Monte Carlo simulations on the basis of 2D Heisenberg Hamiltonian model were carried out, in which the spin Hamiltonian is considered as $H = -\sum_{ij} J_1 S_i S_j - \sum_{ik} J_2 S_i S_k - A S_i^Z S_i^Z$, where J_1 and J_2 are the first and second nearest-neighboring exchange parameters (Figure S6), respectively. S is the spin vector of Mn atom, S^z is the spin component along the z direction, and A is the single-ion magneto crystalline anisotropy arising from spin-orbital coupling. Supercells of 100 × 100 × 1 grids were adopted for MnP and MnAs monolayers. The accurate T_c can be obtained by locating the peak position of magnetic susceptibility, which is calculated at a given temperature. Based on the simple Ising model, the calculated T_c of MnP and MnAs monolayers are estimated to be 745 K and 1050 K (Figure S7), which is likely overestimated. Different from the simple numbers (+1 or -1) on Ising model, the spins on all magnetic sites flip randomly, which are more accurate to estimate the Curie temperature. The energy differences of FM, AFM1, and AFM3 ground states (see Table S2) were used to compute $J_1$and J_2, we have:

$$E(FM) = E_0 - 2J_1|S|^2 - 2J_2|S|^2 - A|S|^2$$

$$E(AFM1) = E_0 + 2J_1|S|^2 - 2J_2|S|^2 - A|S|^2$$

$$E(AFM3) = E_0 + 2J_2|S|^2 - A|S|^2$$

Thus,

$$J_1 = \frac{E(AFM1) - E(FM)}{4|S|^2}$$

$$J_2 = \frac{2E(AFM3) - E(AFM1) - E(FM)}{8|S|^2}$$

Anisotropy energy parameter A is calculated to be 166 μeV and 281 μeV for 2D MnP and MnAs monolayers, respectively.

Table S1. Relative energies ΔE (meV) ($\Delta E=E_{AFM}-E_{FM}$) , magnetic moments μ_B and electronic structures (*ES*) with PBE+U=4 eV and HSE for MnX (X=P, As) monolayers, respectively.

	ΔE (PBE+U)	**ΔE (HSE)**	**μ_B(PBE+U)**	**μ_B(HSE)**	***ES*(PBE+U)**	***ES*(HSE)**
MnP	**53**	**62**	**8**	**8**	**half-metal**	**half-metal**
MnAs	**95**	**87**	**8**	**8**	**half-metal**	**half-metal**

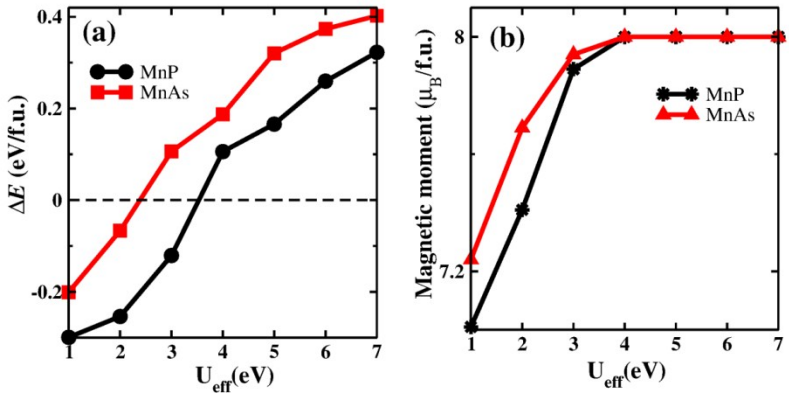

Figure S1. Energy difference ΔE ($\Delta E=E_{AFM}-E_{FM}$) (a) and magnetic moment per unit cell (b) as a function of U_{eff} of MnP and MnAs monolayer.

Figure S1 shows the calculated ΔE($\Delta E=E_{AFM}-E_{FM}$) and magnetic moments (μ_B) using GGA+U method with U_{eff} varied from 0 to 7 eV. As can be seen, ΔE is sensitive to U_{eff} and it increases with the increasing U_{eff}, suggesting that MnP and MnAs monolayers are the strongly correlated system. As we do not have experimental data to exactly define the U_{eff} value, we have to use Heyd-Scuseria-Ernzerhof (HSE06) result to get a proper U_{eff} value. As shown in Table S1, PBE+U with U_{eff}=4.0eV well reproduces the HSE06 results in terms of magnetic ground states, magnetic moments, and electronic structures. In fact, as shown in Figure S1, the FM is more stable than AFM when U is larger than 2.4 eV for MnAs and 3.5 eV for MnP and the magnetic moment saturates to ~8 μ_B around U_{eff}=4eV. Therefore, U_{eff}=4.0 eV was used to treat partially filled *d* orbital of the Mn atom in this work.

2. Four different AFM states

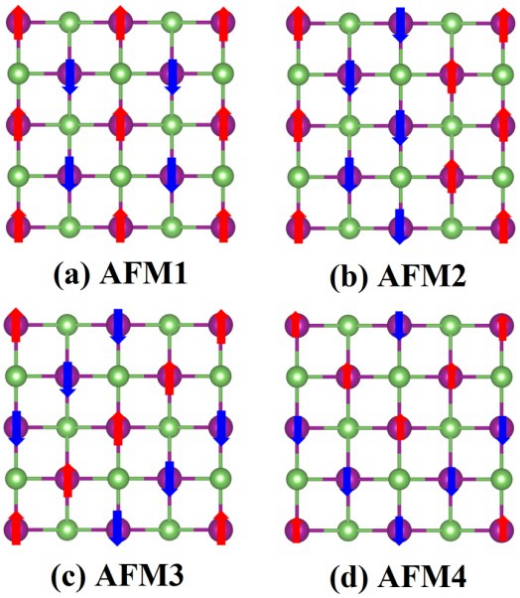

Figure S2. Top views (a−d) of geometric structures four different AFM states for 2D MnX (X = P, As, Sb) monolayers. Red and blue arrows denote two opposite spin orientations.

3. Ground states, lattice parameters, and atomic positions of MnX monolayers

Table S2. Ground states (*GS*), nearest-neighboring (d_N) and second nearest-neighboring (d_{NN}) Mn-Mn bond lengths with the angle (θ_1, θ_2) of Mn-X-Mn (Figure S5), charge transfer (*C*), lattice parameters (*Lattice*) and atomic positions (*Coordinates*) for MnX (X=P, As, Sb) monolayers. The phase of MnP and MnAs monolayer belongs to the tetragonal *P*4/*nmm* space group (No. 129). FM and AFM4 denote ferromagnetic and antiferromagnetic states, respectively.

System	*GS*	d_N (Å)	d_{NN} (Å)	θ_1	θ_2	*C* (*e*)	*Lattice* (Å)	*Coordinates*
MnP	**FM**	**3.13**	**4.42**	**79**	**127**	**0.98**	**a = b= 4.42**	**Mn (0, 0, 0.5)** **P (0.5, 0, 0.457)**
MnAs	**FM**	**3.21**	**4.54**	**77**	**123**	**0.88**	**a = b= 4.53**	**Mn (0, 0, 0.5)** **As (0.5, 0, 0.459)**
MnSb	**AFM4**	**3.31**	**4.67**	**72**	**113**	**0.69**	**a = b= 4.67**	**Mn (0, 0, 0.5)** **Sb (0.5, 0, 0.427)**

4. Relative energies between FM and AFM

Table S3. Relative energies (meV/Mn) between ferromagnetic (FM) and four antiferromagnetic (AFM1, AFM2, AFM3, and AFM4) for MnX (X=P, As, Sb) monolayers. Ground states are highlighted with blue backgrounds.

System	FM	AFM1	AFM2	AFM3	AFM4
MnP	**0**	**52.9**	**238**	**187**	**249**
MnAs	**0**	**95.1**	**197**	**302**	**254**

MnSb	**0**	**188**	**230**	**194**	**-206**

5. Electron localization functions for MnP and MnAs

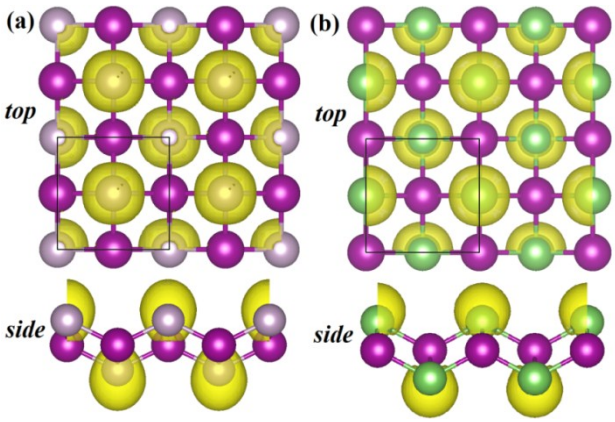

Figure S3. Top and side views of electron localization functions (ELF) for MnP (a), and MnAs (b) monolayers with iso-surface values of 0.5.

6. Evolution of total energy at 300 K

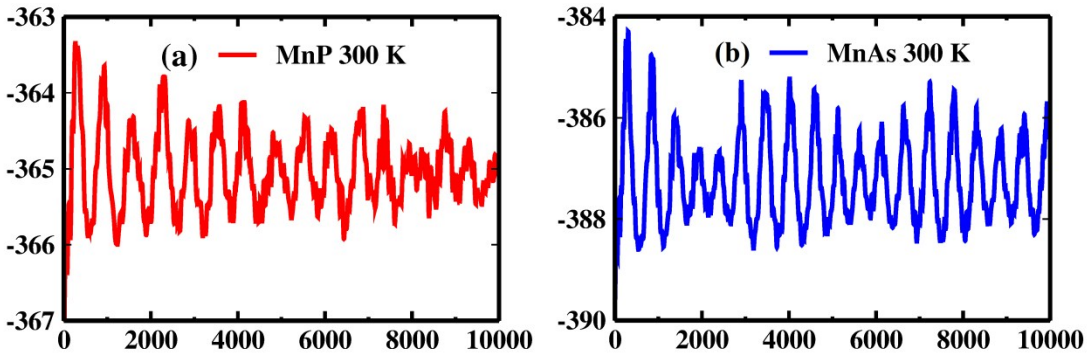

Figure S4. Evolution of total energy of MnP (a) and MnAs (b) with temperature of 300 K.

7. Atom-projected and orbital-projected densities of states

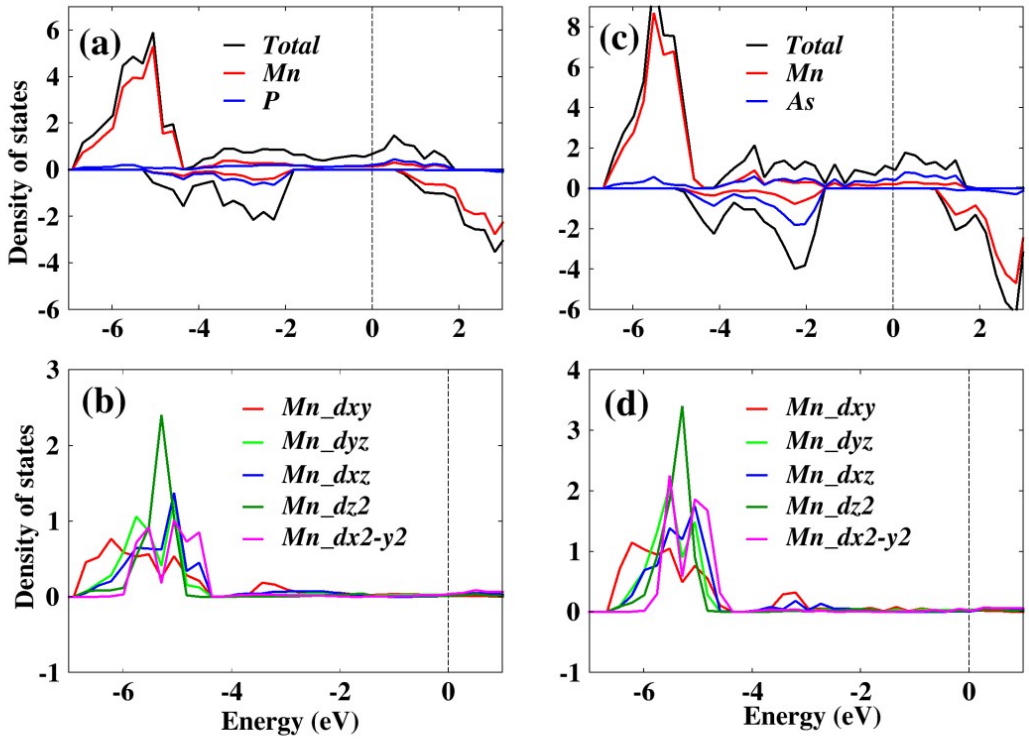

Figure S5. Atom-projected and orbital-projected densities of states for MnP (a,b) and MnAs (c,d) monolayers by using accurate HSE06 hybrid functional, and the Fermi levels are all set to zero.

8. Spin configuration for the exchange-interaction constants.

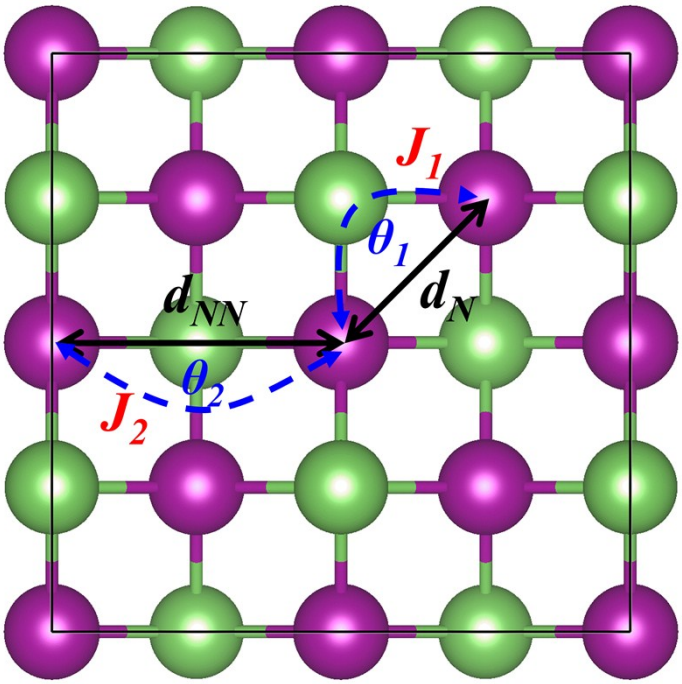

Figure S6. Spin configuration for estimating the exchange-interaction constants. J_1 and J_2 are the nearest and next nearest magnetic exchange interaction parameters, respectively.

9. On-site magnetic moment of Mn atoms and magnetic susceptibility versus temperature

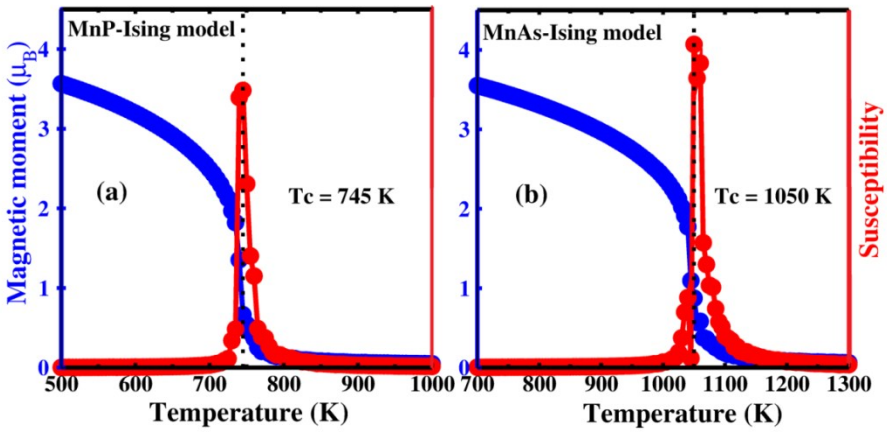

Figure S7. On-site magnetic moment of Mn atoms and magnetic susceptibility versus temperature in MnP (a) and MnAs (b) monolayers based on Ising model.

10. Three relatively low-energy MnX monolayers searched by CALYPSO.

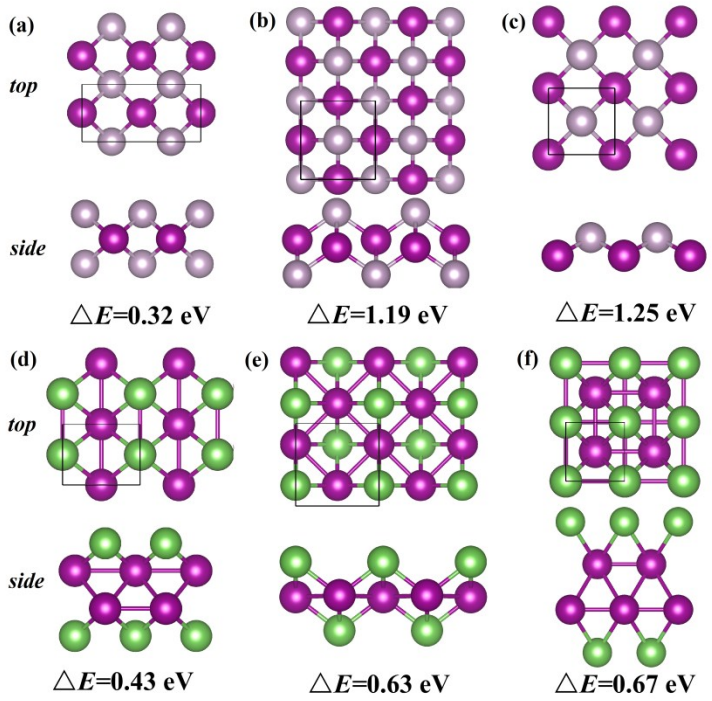

Figure S8. Three relatively low-energy MnP monolayer (a, b, c) and MnAs monolayer (d, e f) searched by CALYPSO**.** Their energies relative (△E) to the lowest energy are also shown.

11. Crystal structure of AMn_2Y_2

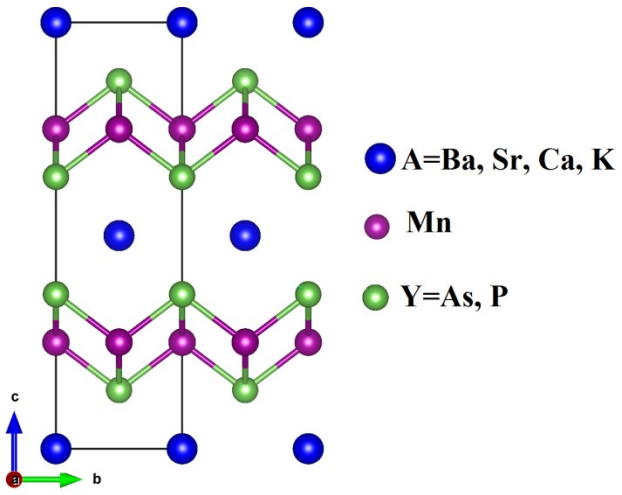

Figure S9. Crystal structure of ternary layered compounds AMn_2Y_2 (A= Ba, Sr, Ca, K, Y=P, As)

12. Bond lengths, exfoliation energy, and elastic constants for bulk $BaMn_2Y_2$

Table S4. The Ba-Y and Mn-Y bond lengths (Å), exfoliation energy E_f (eV/Å^2), and elastic constants C (GPa) for bulk $BaMn_2Y_2$ (Y=P, As).

System	Ba-Y	Mn-Y	E_f	C_{11}	C_{12}	C_{13}	C_{33}	C_{44}	C_{66}
$BaMn_2P_2$	3.45	2.56	0.066	107	21	28	64	22	38
$BaMn_2As_2$	3.53	2.68	0.074	103	17	21	56	21	34

The ternary layered compounds AMn_2Y_2 (A=Ca, Sr, Ba, Y=P, As) have already been synthesized[10-12], in which the MnY layer and A atomic layer are alternatively stacked in the *c*-axis (Figure S9). Take $BaMn_2As_2$ and $BaMn_2P_2$ as the examples, the Ba-Y bond lengths of bulk $BaMn_2Y_2$ are much larger than Mn-Y bond lengths (Table S3), indicating relatively weak strength of Ba-Y bonds.

The exfoliation energy E_f of a bulk AMn_2Y_2 phase into 2D MnY is calculated through $E_f = -[E_{tot(AMn2Y2)} - 2E_{tot(Mn2Y2)} - 2E_{tot(A)}]/(4S)$, where $E_{tot(BaMn2Y2)}$, $E_{tot(Mn2Y2)}$, and $E_{tot(Ba)}$ stand for the total energies of bulk $BaMn_2Y_2$ phase, 2D MnY, and A element, respectively and S is the surface area. Exfoliating a MnY phase, each unit cell of the AMn_2Y_2 phase generates two MnY layers with 4 surfaces. Therefore, the exfoliation energy is divided by 4 in one unit cell. The exfoliation energy of MnP (0.066 eV/Å^2) and MnAs (0.074 eV/Å^2) monolayers are all lower than those of most MXenes (0.086~0.205 eV/Å^2), which have a better chance to be exfoliated into MnY monolayer. The relatively low interlayer exfoliation energies suggest that these monolayers could be easily obtained from their bulk structures. Besides, C_{11} and C_{33} elastic constants (Table S3) are kinds of quantities that imply the stiffness of overall chemical bonds along the *ab* and *c* directions, respectively. As a result, C_{11} is obviously much larger than C_{33}, suggesting it might be more feasible to break the Ba-Y bonds under appropriate mechanical and chemical tensions without significantly damaging the Mn-Y bonds. As analysis above, MnY synthesis may be achieved by selective etching of the A element layers and possible from their bulk AMn_2Y_2 phases (Figure 4e).

13. Three AFM orders and Band structures of MnP and MnAs bilayer

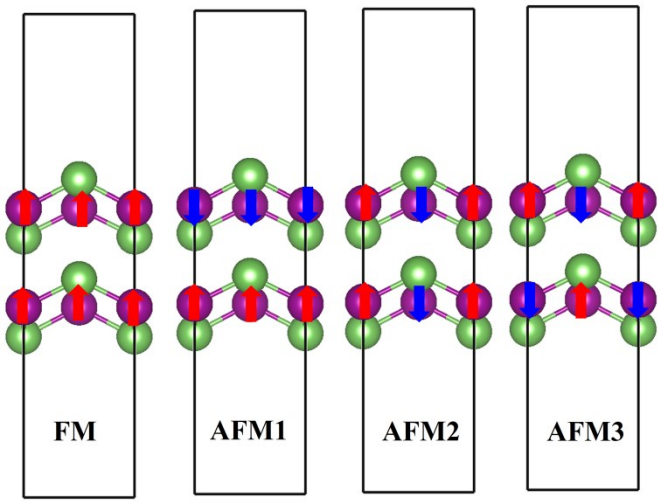

Figure S10. Side views of FM and three different AFM states for 2D MnX (X = P, As) bilayers. Red and blue arrows denote two opposite spin orientations.

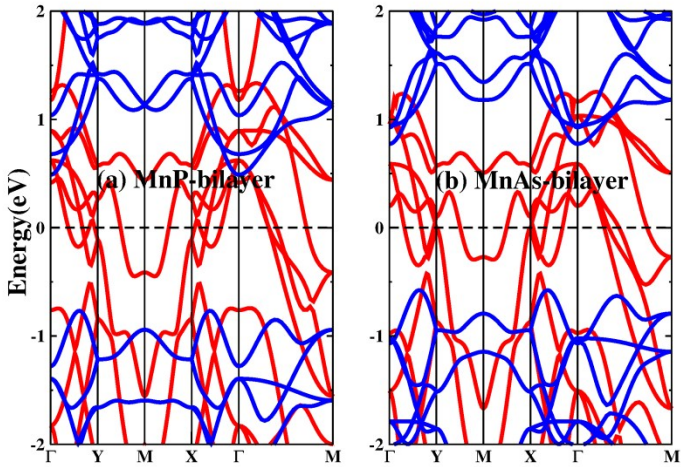

Figure S11. Band structures of MnP (a) and MnAs (b) bilayer at PBE+U level. The red and blue lines represent spin-up and spin-down, respectively.

We also have investigated the spin order of bilayer structures of MnP and MnAs bilayer carefully. Three AFM spin orders are considered of MnP and MnAs bilayer shown in Figure S10. Interestingly, the ferromagnetism and half-metallicity can be well preserved in MnP and MnAs bilayer. The band structures for bilayer are shown in Figure S11.

References

1. Wang, Y.; Lv, J.; Zhu, L.; Ma, Y., *Phys. Rev. B* **2010,** *82*, 094116.
2. Wu, Q.; Xu, W. W.; Qu, B.; Ma, L.; Niu, X.; Wang, J.; Zeng, X. C., *Mater. Horiz.* **2017**, *4*, 1085-1091.
3. Wang, B.; Yuan, S.; Li, Y.; Shi, L.; Wang, J., *Nanoscale* **2017**, *9*, 5577.
4. Wang, Y.; Li, F.; Li, Y.; Chen, Z., *Nat. Commun.* **2016,** *7*, 11488.
5. Ma, F.; Jiao, Y.; Gao, G.; Gu, Y.; Bilic, A.; Chen, Z.; Du, A., *Nano Lett.* **2016,** *16*, 3022-8.

6. Luo, X.; Yang, J.; Liu, H.; Wu, X.; Wang, Y.; Ma, Y.; Wei, S. H.; Gong, X.; Xiang, H., *J. Am. Chem. Soc.* **2011,** *133*, 16285.
7. An, J.; Sefat, A. S.; Singh, D. J.; Du, M.-H., *Phys. Rev. B* **2009,** *79*, 075120.
8. Nath, R.; Singh, Y.; Johnston, D. C., *Phys.Rev. B* **2009,** *79*, 174513.
9. Li, H., *EPL (Europhysics Letters)* **2012,** *99*, 17007.